Applied Surface Science 467–468 (2019) 249–254

Contents lists available at ScienceDirect

Applied Surface Science

journal homepage: www.elsevier.com/locate/apsusc

Full Length Article

Effects of thermal treatment on optoelectrical properties of AZO/Ag-Mg-Al thin films

H.K. Lin*, B.F. Chung

Graduate Institute of Materials Engineering, National Pingtung University of Science and Technology, 1, Hseuhfu Road, Pingtung 912, Taiwan

ARTICLE INFO

Keywords:
Metallic glass
Transparent conductive film
Laser
Annealing

ABSTRACT

AgMgAl films with a thickness of 6–12 nm were deposited on glass substrates using a co-sputtering process. AZO layers were then deposited on the AMA films to form bi-layer structures. The films were processed by traditional furnace annealing at temperatures of 100–200 °C and laser annealing with a laser power of 25–800 mW and repetition rates ranging from 100 to 400 kHz. For the non-annealed samples, the sheet resistance reduced and the transmittance increased with the addition of the AZO film to the AMA layer. For the optimal AMA thickness of 12 nm, the sheet resistance was equal to 85 Ω/□, while the transmittance was equal to 74%. According to the DSC results, the crystallization temperature of the AMA film was around 100–150 °C. Following furnace annealing, the optoelectrical properties of the bi-layer structure improved due to the crystallization of the AMA film. Furthermore, for the laser-annealed film processed using a pulse energy of 0.5 μJ and a repetition rate of 400 kHz, the sheet resistance was reduced to 45 Ω/□, while the transmittance was improved to 87%.

1. Introduction

Transparent conducting oxide (TCO) films are used in many electrical applications due to their high transparency and good electrical conductivity [1,2]. Indium-tin oxide (ITO) film has particularly good electrical and optical properties and is thus commonly used as an electrode material [3–5]. The thickness of ITO films should exceed 100 nm in order to minimize the sheet resistance [6,7]. Consequently, many proposals have been presented for minimizing the use of ITO by means of specially designed structures, new materials, and optimized sputtering processes [8–11]. Typically, ITO-based multilayer structures incorporate a metal middle layer with a thickness of approximately 5–20 nm to increase the electrical conductivity and improve the transmittance [10–16].

ZnO films have many advantages for electrical applications, including non-toxicity, high stability in hydrogen plasma processes, low temperature growth, and good scalability [3]. As a result, ZnO is an attractive alternative to ITO as an electrode material. Notably, many studies have shown that the electrical resistivity of ZnO thin films can be enhanced through the addition of impurities (e.g., Al) using techniques such as atomic layer deposition (ALD) [17], ion beam sputter deposition (IBSD) [18], sol gel [19,20], spin coating [21], chemical spray pyrolysis [22] and magnetron sputtering [23,24].

Thin film metallic glasses (TFMGs) have excellent mechanical strength, good anti-corrosion resistance, and a high bending fatigue strength [25–27]. Furthermore, they exhibit a lower surface roughness than pure metallic films and have a higher nucleation rate. As a result, they can be prepared with a thickness much lower than that of the metal layers used in traditional ITO sandwich structures. Finally, TFMGs have excellent transparency and conductivity properties [28]. Consequently, they have been extensively used in the industrial, electronics and bio-medicine fields in recent years. Lee et al. [29] prepared a bi-layer ITO/ZrCu film with a continuous and smooth ZrCu layer and a thickness of less than 6 nm using a magnetron sputtering process conducted under room temperature conditions. The ZrCu film was shown to have an optical transmittance of 73% and a sheet resistance of 20 Ω/sq. Lin [30] reported that the AgMgAl thin films, in an attempt in replacing the expensive pure Au contact films, are prepared by co-sputtering. Appropriate short thermal annealing for the amorphous films can drastically lower the resistivity down to as low as 9 μΩ-cm. The AgMgAl films would be much cheaper than the pure Au films, favorable for industry applications. In a later study, the authors replaced the ZrCu film with an AAM film [31]. However, the results showed that the film had a slightly lower optical transmittance (65%) and a significantly higher electrical resistivity (90 Ω/□). Moreover, the CuZr film was also replaced by the CuMg film and it showed that the bi-layer ITO/CuMg structure improved the transmittance from 53% (ITO/CuZr) to 75.6% (ITO/CuMg) and reduces the resistance from 140 Ω/□ (ITO/

* Corresponding author.
E-mail address: HKLin@mail.npust.edu.tw (H.K. Lin).

https://doi.org/10.1016/j.apsusc.2018.10.135
Received 27 June 2018; Received in revised form 1 October 2018; Accepted 15 October 2018
Available online 20 October 2018
0169-4332/

CuZr) to 49.5 Ω/□ (ITO/CuMg) [32].

Many studies have shown that the optical and electrical properties of thin films can be improved through annealing [2,33–37]. As a result, the literature contains many proposals for the localized annealing of TCO films using thermal processing or laser irradiation [38–43]. For example, Vernieuwe et al. [44] printed AZO films were on glass substrates in non-vacuum conditions and heated the films in a tube furnace to a temperature of 500 °C under an O_2/N_2 atmosphere. The resulting films were found to have an electrical resistivity of 2.54×10^{-2} Ω/cm were obtained. Xu [45] deposited AZO thin films on quartz substrates using an RF magnetron sputtering system and then annealed the films using a solid-state laser with a power density of 27.8 W/mm^2. The annealed films had a good quality crystallized structure, obvious grain boundaries, and no surface damage. Moreover, the carrier concentration, mobility and resistivity were all significantly improved following annealing, while the transmittance was around 90% in the visible region. It was shown in [31] that the optical and electrical properties of ITO/AMA thin films can be improved through laser annealing with a repetition rate of 400 kHz and a pulse energy of 1.03 μJ. However, ITO is a relatively high-cost material and is available only in finite quantities.

Accordingly, in this study, the ITO film is replaced with a cheaper AZO film. The effects of the AMA thickness and annealing conditions (furnace annealing or laser irradiation) on the optoelectrical properties of the AZO/AMA films are investigated using spectrophotometry, four-point probe, differential scanning calorimetry (DSC), scanning electron microscopy (SEM), transmission electron microscopy (TEM) and X-ray diffraction (XRD) techniques.

2. Experimental

Ag-Mg-Al (AMA) films with thicknesses of 6–12 nm were deposited on glass substrates using a co-sputtering process with Ag, Mg and Al target powers of 60, 70 and 70 W, respectively. AZO layers with a thickness of 50 nm were then deposited on the AMA films using an AZO target power of 55 W. The composition of the AMA films was found from EDX analysis to be $Ag_{40}Mg_{40}Al_{20}$. AMA and AZO/AMA (AAMA) films were annealed using a traditional furnace technique at temperatures ranging from 100 to 200 °C for 1 h. AMA and AAMA films were additionally annealed using a pulse laser with a wavelength of 1064 nm, a spot size of 40 μm and a scanning speed of 5 mm/s. In performing the annealing process, the repetition rate was varied in the range of 100–400 kHz and the laser power was set as 25–800 mW. For each annealing process, the pulse energy (E) was computed as [46]

$$E = P_{AVG}/rep, \quad (1)$$

where P_{AVG} is the average power of the pulse laser and rep is the laser repetition rate. For the irradiation powers and repetition rates considered in the present study, the pulse energy varied in the range of 0.25–2 μJ.

The crystallization behavior of the AMA films and the thermal property was measured using a differential scanning calorimeter (Diamond, PerkinElmer). In this study, the DSC technique with a heating rate of 5 °C/min was carried out for AMA layer and a temperature range of 30–200 °C. The morphologies and compositions of the as-deposited and annealed AMA and AAMA films were examined by scanning electron microscopy (SEM, JSM-7600F), X-ray diffraction (XRD, Bruker D8 Advance) and transmission electron microscopy (TEM, JEM-3010). The optical transmittance of the films was measured using a UV–vis-IR spectrophotometer (Lambda 35, PerkinElmer). Finally, the sheet resistance was measured using a four-point probe (SR-H1000C).

3. Results and discussion

Fig. 1 shows the XRD pattern of the as-deposited $Ag_{40}Mg_{40}Al_{20}$ film. The absence of any distinct diffraction peaks indicates that the film has an amorphous structure. Fig. 2 shows the variation of the sheet resistance with the AMA film thickness for the AMA and AAMA samples. For both samples, the sheet resistance reduces with an increasing AMA thickness due to a greater continuity of the film structure and the sheet resistance stabilizes at an AMA thickness greater than 12 nm. The AMA monolithic film with a thickness of 12 nm has a sheet resistance of 90 Ω/sq. However, following the deposition of the AZO film on the AMA layer, the sheet resistance reduces to 85 Ω/sq. This finding is consistent with the parallel electrical resistance circuit model of bi-layer films and reflects the fact that the bottom AMA film has a lower electrical resistance than the upper AZO layer [47].

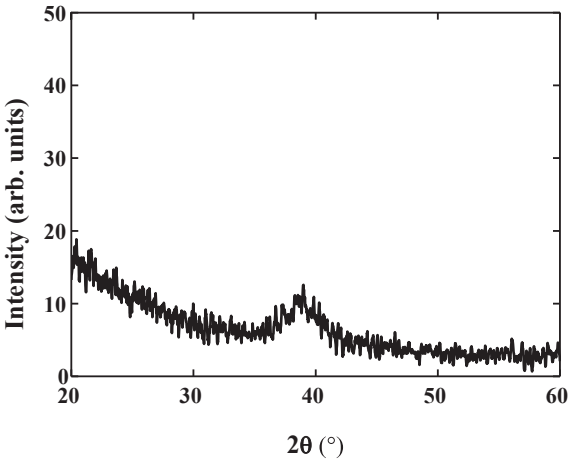

Fig. 1. XRD pattern of as-deposited AMA film.

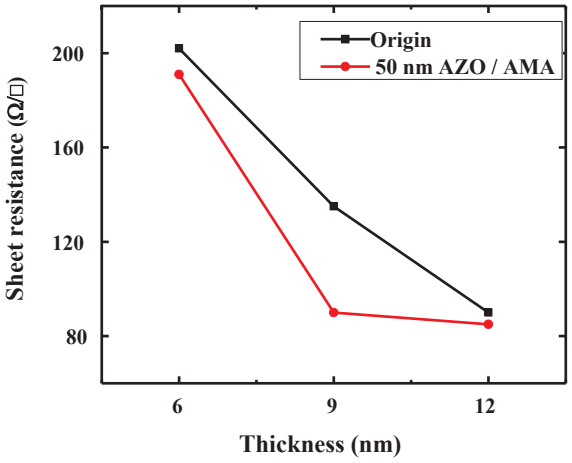

Fig. 2. Sheet resistance of AMA and AAMA films as function of AMA film thickness.

Fig. 3 shows the variation of the transmittance with the AMA film thickness for the AMA and AAMA samples. It is seen that the transmittance of the AMA films increases following the deposition of the AZO layer. However, for both the AMA films and the AAMA films, the transmittance reduces with an increasing AMA thickness due to the greater reflectivity of the AMA layer. Overall, the results presented in Figs. 2 and 3 show that the electrical resistivity reduces with an increasing AMA film thickness, whereas the transmittance increases with a reducing AMA thickness. Observing the two figures, the optimal AMA thickness is found to be 12 nm, for which the electrical resistivity of the AAMA sample is equal to 85 Ω/□, while the optical transmittance is 74%.

In an attempt to improve the optoelectrical properties of the AAMA samples, the films were annealed under various temperatures (furnace annealing) and pulse energies and repetition rates (laser irradiation).

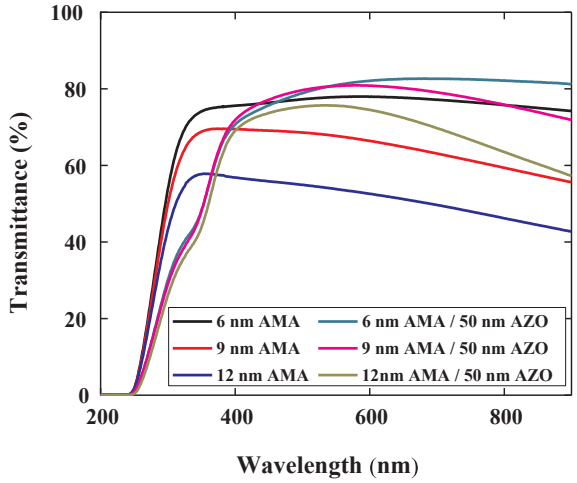

Fig. 3. Optical transmittance of AMA and AAMA films as function of AMA film thickness.

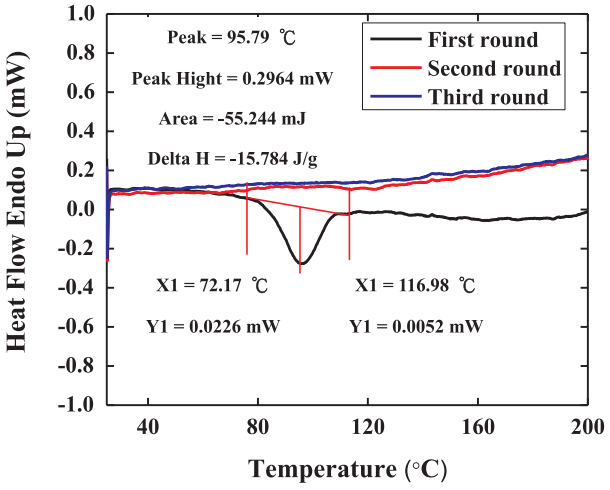

Fig. 4. DCS results for as-deposited AMA film tested using heating rate of 5 °C/min.

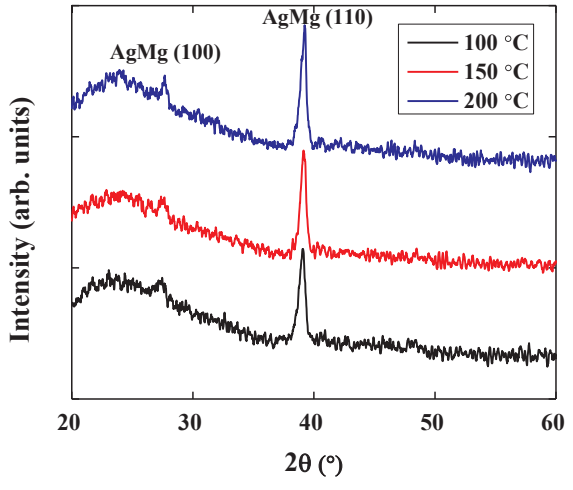

Fig. 5. XRD patterns of AMA films annealed at different temperatures.

The DSC results shown in Fig. 4 indicate that the AAMA material undergoes an enthalpy change (H) of 15.78 J/g at a temperature of approximately 72–116 °C. Fig. 5 presents the XRD analysis results for AMA films with a thickness of 100 nm annealed at temperatures of 100, 150 and 200 °C, respectively. All of the XRD patterns contain prominent peaks corresponding to the (1 0 0) and (1 1 0) orientations. In other words, the results confirm that the AMA films have a crystalline structure following annealing at temperatures higher than 100 °C.

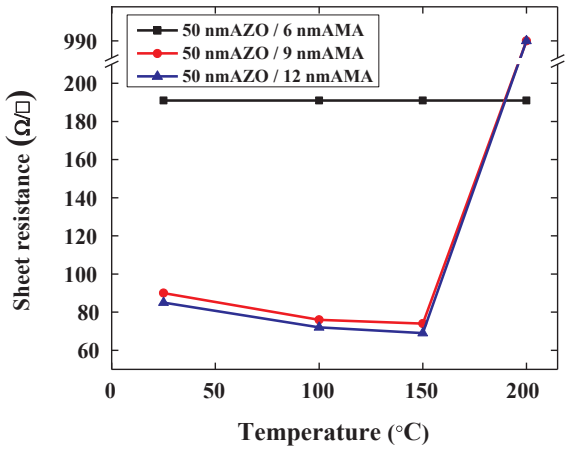

Fig. 6. Sheet resistance of AAMA films annealed at various temperatures.

Fig. 6 shows the sheet resistance values of the AAMA samples with different AMA thicknesses following furnace annealing at various temperatures in the range of 100–200 °C. The sheet resistance of the AAMA sample with a 6-nm AMA film is insensitive to the annealing temperature. However, for AMA film thicknesses of 9 nm and 12 nm, respectively, the sheet resistance reduces as the annealing temperature is increased toward 150 °C and then increases sharply as the temperature is further increased to 200 °C. The minimum sheet resistance of the AAMA film is equal to approximately 69 Ω/□. In other words, the annealing process reduces the resistance of the AAMA film by around 18.8%. The optimal annealing temperature of 150 °C is consistent with the DSC results presented in Fig. 4, which shows that amorphous AMA film became crystallized film.

Fig. 7 shows the optical transmittance of the AAMA films annealed at 150 °C. It is seen that the transmittance of the AAMA sample with an AMA thickness of 12 nm increases from around 74% in the as-deposited condition (Fig. 3) to 82% after the annealing process. In other words, the annealing process not only reduces the sheet resistance (Fig. 6), but also improves increases the transmittance. The annealing process improves the transmittance by around 9% compared to the as-deposited sample.

Fig. 8(a) and (b) show the SEM surface morphologies of the AAMA samples with an AMA thickness of 12 nm annealed at 100 °C and 200 °C, respectively. As indicated by the XRD results in Fig. 5, the

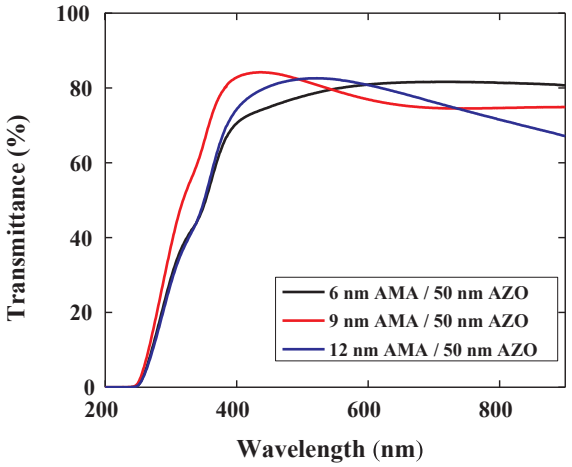

Fig. 7. Optical transmittance of AAMA films annealed at 150 °C.

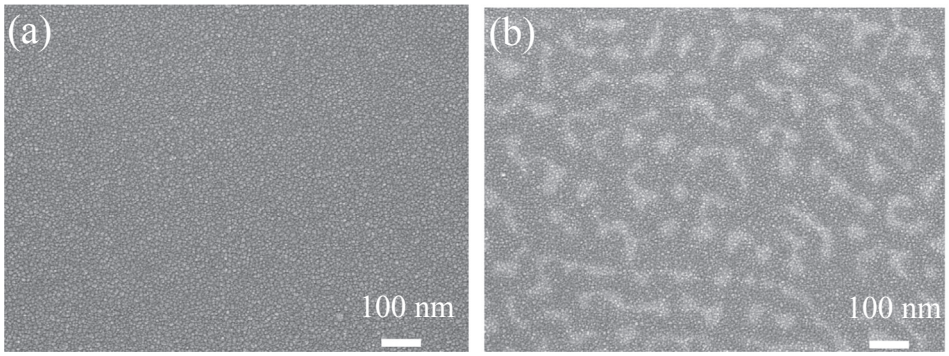

Fig. 8. SEM surface morphologies of AAMA films annealed at: (a) 100 °C and (b) 200 °C.

microstructure of the AAMA film transforms to a fine crystalline structure following annealing at a temperature of 100 °C (Fig. 8(a)). The dense microstructure results in a greater scattering of the conduction electrons [43]. Consequently, the sheet resistance reduces compared to that of the as-deposited sample. Furthermore, the refractive index of the AAMA structure is also reduced, and consequently the transmittance increases. However, at a higher temperature of 200 °C, the film surface contains island-like structures (Fig. 8(b)). As a result, the electrical conductivity is significantly increased due to a discontinuous film. It showed that the AAMA film annealed at 200 °C and the sheet resistance increased up to 990 Ω/□ (Fig. 6).

Fig. 9 shows the sheet resistance and transmittance properties of the AAMA samples with a 12-nm AMA film following laser annealing with different pulse energies and repetition rates. As discussed earlier in relation to Fig. 3, the as-deposited AAMA sample has a sheet resistance of 85 Ω/□. However, Fig. 9 shows that the sheet resistance reduces significantly following laser annealing. For example, a minimum sheet resistance of 32 Ω/□ is obtained when using a pulse energy of 1.5 μJ and a repetition rate of 100 kHz. As the pulse energy reduces, the sheet resistance increases. However, the transmittance is significantly improved; particularly at higher repetition rates. Overall, the results show that the optimal irradiation conditions are a pulse energy of 0.5 μJ and a repetition rate of 400 kHz, which lead to a sheet resistance of 45 Ω/□ and a transmittance of 87%. The new structure achieves the better optical property and the optimal transmittance increases by 8.7% in this study compared with our previous result [31]. Particularly, an AZO film replaces ITO film because ITO film is a relatively high-cost material and is available only in finite quantities.

Fig. 10(a) presents a cross-sectional TEM image of the annealed AAMA sample processed using a pulse energy of 1 μJ and a repetition rate of 400 kHz. The thickness of the crystal-AMA structure is found to be the same as that of the as-deposited amorphous-AMA thin film, i.e.,

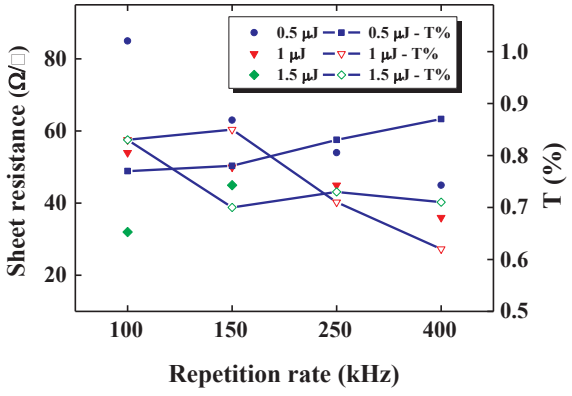

Fig. 9. Sheet resistance and transmittance of AAMA samples with 12-nm thick AMA film following laser annealing with various pulse energies and repetition rates.

12 nm. In other words, the irradiated laser energy is sufficient to fully crystallize the amphous-AMA thin film. However, the continuous film transforms to an island-like structure following the annealing process (see Fig. 10(b)). In particular, the microstructure resembles that of the sample furnace annealed at a high temperature of 200 °C (see Fig. 8(b)). The high-resolution TEM image presented in Fig. 10(b) shows that the sample has a periodic atomic structure. Finally, the electron diffraction pattern presented in Fig. 10(c) confirms that the AMA sample has a crystalline structure with a strong (1 1 0) orientation, as indicated previously by the XRD results. As a result, the electrical conductivity is significantly increased due to a discontinuous film. Therefore, the better electric and optical properties of the AMA samples are achieved at an appropriate condition. In the study, DSC and TEM results show important evidence to the optimal annealing condition.

The performance of AAMA films with known sheet resistance and transmittance properties can be compared using the following figure of merit [48]:

$$\Psi_{TC} = T^{10}/R, \quad (2)$$

where T is the transmittance and R is the sheet resistance. Substituting the transmittance and sheet resistance values of the AAMA sample annealed with a laser repetition rate of 400 kHz and a pulse energy of 0.5 μJ (i.e., 87% and 45 Ω/□, respectively) into Eq. (2), the optimal figure of merit is found to be $5.5 \times 10^{-3}\ \Omega^{-1}$. The FOM of the non-annealed sample is $5.8 \times 10^{-4}\ \Omega^{-1}$ (i.e., 74% and 85 Ω/□, respectively). Therefore, the figure of merit value is improved by annealing process.

4. Conclusion

Bi-layer AZO/AMA metallic glass films have been deposited on glass substrates using a co-sputtering process. The films were processed by furnace annealing at temperatures of 100 to 200 °C for 1 h and laser annealing with repetition rates in the range of 100–400 kHz and laser powers ranging from 25 to 800 mW. The results have shown that the as-deposited bi-layer structure has a sheet resistance of 85 Ω/□ and an optical transmittance of 74% given AZO and AMA layer thicknesses of 50 nm and 12 nm, respectively. The DSC and XRD results have shown that the amorphous structure of the as-deposited samples transforms to a crystalline structure under high annealing temperatures (100 °C) and laser pulse energies (0.5 μJ). The crystalline structure results in a significant improvement in the optoelectrical properties of the bi-layer sample. The optimal values of the optical transmittance and sheet resistance are found to be 87% and 45 Ω/□, respectively, given a pulse energy of 0.5 μJ.

Acknowledgement

The authors gratefully acknowledge the financial support provided to this study by the Ministry of Science and Technology of Taiwan

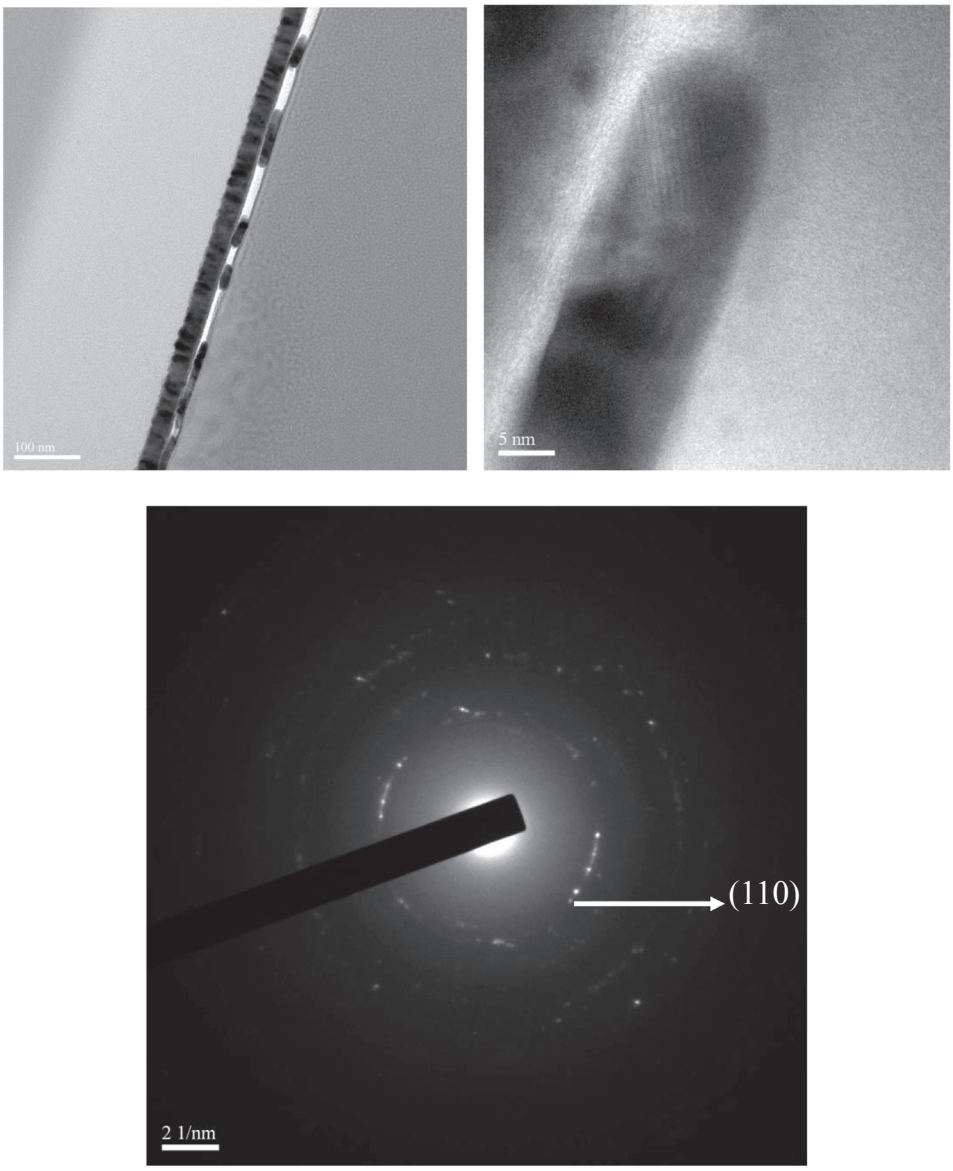

Fig. 10. (a) Cross-sectional TEM image, (b) high-resolution TEM image, and (c) diffraction pattern of AAMA film following laser annealing with pulse energy of 1 μJ and repetition rate of 400 kHz.

under Grant Nos. MOST 103-2221-E-020-010 and 103-2120-M-110 -004.

References

[1] H.K. Lin, C.H. Li, S.H. Liu, Patterning electrode for cholesteric liquid crystal display by pulsed laser ablation, Opt. Lasers Eng. 48 (2010) 1008–1011.
[2] S.J. Wakeham, M.J. Thwaites, B.W. Holton, C. Tsakonas, W.M. Cranton, D.C. Koutsogeorgis, R. Ranson, Low temperature remote plasma sputtering of indium tin oxide for flexible display applications, Thin Solid Films 518 (2009) 1355–1358.
[3] C.W. Yang, J.W. Park, The cohesive crack and buckle delamination resistances of indium tin oxide (ITO) films on polymeric substrates with ductile metal interlayers, Surf. Coat. Technol. 204 (2010) 2761–2766.
[4] X. Liu, X. Cai, J. Mao, C. Jin, ZnS/Ag/ZnS nano-multilayer films for transparent electrodes in flat display application, Appl. Surf. Sci. 183 (2001) 103–110.
[5] J.A. Jeong, H.K. Kim, Low resistance and highly transparent ITO–Ag–ITO multilayer electrode using surface plasmon resonance of Ag layer for bulk-heterojunction organic solar cells, Sol. Energy Mater. Sol. Cells 93 (2009) 1801–1809.
[6] C. Guillén, J. Herrero, Comparison study of ITO thin films deposited by sputtering at room temperature onto polymer and glass substrates, Thin Solid Films 480–481 (2005) 129–132.
[7] J. Lee, H. Jung, J. Lee, D. Lim, K. Yang, J. Yi, W.C. Song, Growth and characterization of indium tin oxide thin films deposited on PET substrates, Thin Solid Films 516 (2008) 1634–1639.
[8] H. Park, S. Qamar Hussain, S. Velumani, A.H. Tuan Le, S. Ahn, S. Kim, J. Yi, Influence of working pressure on the structural, optical and electrical properties of sputter deposited AZO thin films, Mater. Sci. Semicond. Process. 37 (2015) 29–36.
[9] K.H. Patel, S.K. Rawal, Influence of power and temperature on properties of sputtered AZO films, Thin Solid Films 620 (2016) 182–187.
[10] T.H. Kim, S.H. Park, D.H. Kim, Y.C. Nah, H.K. Kim, Roll-to-roll sputtered ITO/Ag/ITO multilayers for highly transparent and flexible electrochromic applications, Sol. Energy Mater. Sol. Cells 160 (2017) 203–210.
[11] C. Guillén, J. Herrero, ITO/metal/ITO multilayer structures based on Ag and Cu metal films for high-performance transparent electrodes, Sol. Energy Mater. Sol. Cells 92 (2008) 938–941.
[12] M. Bendera, W. Seeliga, C. Daubeb, H. Frankenbergerb, B. Ockerb, J. Stollenwerkb, Dependence of film composition and thicknesses on optical and electrical properties of ITO–metal–ITO multilayers, Thin Solid Films 326 (1998) 67–71.
[13] K.H. Choi, J.Y. Kim, Y.S. Lee, H.J. Kim, ITO/Ag/ITO multilayer films for the application of a very low resistance transparent electrode, Thin Solid Films 341 (1999) 152–155.
[14] A. Kloppel, B. Meyer, J. Trube, Influence of substrate temperature and sputtering atmosphere on electrical and optical properties of double silver layer systems, Thin Solid Films 392 (2001) 311–314.
[15] A. Indluru, T.L. Alford, Effect of Ag thickness on electrical transport and optical properties of indium tin oxide-Ag-indium tin oxide multilayers, J. Appl. Phys. 105 (2009) 123528.
[16] C. Guillén, J. Herrero, TCO/metal/TCO structures for energy and flexible electronics, Thin Solid Films 520 (2011) 1–17.

[17] L. Ponsonnet, K. Reybier, N. Jaffrezic, V. Comte, C. Lagneau, M. Lissac, C. Martelet, Relationship between surface properties (roughness, wettability) of titanium and titanium alloys and cell behaviour, Mater. Sci. Eng., C 23 (2003) 551–560.
[18] Y.Y. Chen, P.W. Wang, J.C. Hsu, C.Y. Lee, Post-annealing properties of aluminum-doped zinc oxide films fabricated by ion beam co-sputtering, Vacuum 87 (2013) 227–231.
[19] K.E. Lee, M. Wang, E.J. Kim, S.H. Hahn, Structural, electrical and optical properties of sol–gel AZO thin films, Curr. Appl Phys. 9 (2009) 683–687.
[20] S. Chen, M.E.A. Warwick, R. Binions, Effects of film thickness and thermal treatment on the structural and opto-electronic properties of Ga-doped ZnO films deposited by sol–gel method, Sol. Energy Mater. Sol. Cells 137 (2015) 202–209.
[21] Ü.Ö.A. Arıer, B.Ö. Uysal, Effects of precursor parameters on the optical and electrical properties of AZO nano-composite films, Optik – Int. J. Light Electron Opt. 127 (2016) 5065–5069.
[22] C.N. Elias, Y. Oshida, J.H. Lima, C.A. Muller, Relationship between surface properties (roughness, wettability and morphology) of titanium and dental implant removal torque, J. Mech. Behav. Biomed. Mater. 1 (2008) 234–242.
[23] S. Pat, R. Mohammadigharehbagh, S. Özen, V. Şenay, H.H. Yudar, Ş. Korkmaz, The Al doping effect on the surface, optical, electrical and nanomechanical properties of the ZnO and AZO thin films prepared by RF sputtering technique, Vacuum 141 (2017) 210–215.
[24] H.J. Cho, S.U. Lee, B. Hong, Y.D. Shin, J.Y. Ju, H.D. Kim, M. Park, W.S. Choi, The effect of annealing on Al-doped ZnO films deposited by RF magnetron sputtering method for transparent electrodes, Thin Solid Films 518 (2010) 2941–2944.
[25] J.P. Chu, J.C. Huang, J.S.C. Jang, Y.C. Wang, P.K. Liaw, Thin film metallic glasses: preparations, properties, and applications, JOM 62 (2010) 19–24.
[26] J.C. Huang, J.P. Chu, J.S.C. Jang, Recent progress in metallic glasses in Taiwan, Intermetallics 17 (2009) 973–987.
[27] J.P. Chu, J.S.C. Jang, J.C. Huang, H.S. Chou, Y. Yang, J.C. Ye, Y.C. Wang, J.W. Lee, F.X. Liu, P.K. Liaw, Y.C. Chen, C.M. Lee, C.L. Li, C. Rullyani, Thin film metallic glasses: Unique properties and potential applications, Thin Solid Films 520 (2012) 5097–5122.
[28] C.W. Chu, J.S.C. Jang, G.J. Chen, S.M. Chiu, Characteristic studies on the Zr-based metallic glass thin film fabricated by magnetron sputtering process, Surf. Coat. Technol. 202 (2008) 5564–5566.
[29] C.J. Lee, H.K. Lin, S.Y. Sun, J.C. Huang, Characteristic difference between ITO/ZrCu and ITO/Ag bi-layer films as transparent electrodes deposited on PET substrate, Appl. Surf. Sci. 257 (2010) 239–243.
[30] Y.T. Lin, Y.L. Chung, Z.K. Wang, J.C. Huang, AgMgAl metallic glassy and intermetallic thin films for electric contact applications, Intermetallics 57 (2015) 133–138.
[31] H.K. Lin, K.C. Cheng, J.C. Huang, Effects of laser annealing parameters on optical and electrical properties of ITO/metallic glass alloy Bi-layer films, Nanoscale Res. Lett. 10 (2015) 982.
[32] H.K. Lin, S.Z. Hong, Effects of Mg content and annealing treatment on optical and electrical properties of CuMg and ITO/CuMg metallic glass films, J. Alloy. Compd. 731 (2018) 248–252.
[33] H. Morikawa, M. Fujita, Crystallization and electrical property change on the annealing of amorphous indium-oxide and indium-tin-oxide thin films, Thin Solid Films 359 (2000) 61–67.
[34] I.Y.Y. Bu, A simple annealing process to obtain highly transparent and conductive indium doped tin oxide for dye-sensitized solar cells, Ceram. Int. 40 (2014) 3445–3451.
[35] M. Goudarzi, N. Mir, M. Mousavi-Kamazani, S. Bagheri, M. Salavati-Niasari, Biosynthesis and characterization of silver nanoparticles prepared from two novel natural precursors by facile thermal decomposition methods, Sci. Rep. 6 (2016) 32539.
[36] M. Salavati-Niasari, F. Mohandes, F. Davar, K. Saberyan, Fabrication of chain-like Mn2O3 nanostructures via thermal decomposition of manganese phthalate coordination polymers, Appl. Surf. Sci. 256 (2009) 1476–1480.
[37] F. Davar, M. Salavati-Niasari, Synthesis and characterization of spinel-type zinc aluminate nanoparticles by a modified sol–gel method using new precursor, J. Alloy. Compd. 509 (2011) 2487–2492.
[38] S.M.D. Nicolás, D. Muñoz, C. Denis, J.F. Lerat, T. Emeraud, Optimisation of ITO by excimer laser annealing for a-Si:H/c-Si solar cells, Energy Procedia 27 (2012) 586–591.
[39] M.F. Chen, K.M. Lin, Y.-S. Ho, Laser annealing process of ITO thin films using beam shaping technology, Opt. Lasers Eng. 50 (2012) 491–495.
[40] H. Lu, Y. Tu, X. Lin, B. Fang, D. Luo, A. Laaksonen, Effects of laser irradiation on the structure and optical properties of ZnO thin films, Mater. Lett. 64 (2010) 2072–2075.
[41] C.J. Lee, H.K. Lin, C.H. Li, L.X. Chen, C.C. Lee, C.W. Wu, J.C. Huang, A study on electric properties for pulse laser annealing of ITO film after wet etching, Thin Solid Films 522 (2012) 330–335.
[42] H.K. Lin, W.C. Hsu, Electrode patterning of ITO thin films by high repetition rate fiber laser, Appl. Surf. Sci. 308 (2014) 58–62.
[43] F. Wang, M.Z. Wu, Y.Y. Wang, Y.M. Yu, X.M. Wu, L.J. Zhuge, Influence of thickness and annealing temperature on the electrical, optical and structural properties of AZO thin films, Vacuum 89 (2013) 127–131.
[44] K. Vernieuwe, D. Cuypers, C.E.A. Kirschhock, K. Houthoofd, H. Vrielinck, J. Lauwaert, J. De Roo, J.C. Martins, I. Van Driessche, K. De Buysser, Thermal processing of aqueous AZO inks towards functional TCO thin films, J. Alloy. Compd. 690 (2017) 360–368.
[45] F. Ruffino, P. Maugeri, G. Cacciato, M. Zimbone, M.G. Grimaldi, Metal nanostructures with complex surface morphology: The case of supported lumpy Pd and Pt nanoparticles produced by laser processing of metal films, Physica E 83 (2016) 215–226.
[46] B.R. Benware, C.D. Macchietto, C.H. Moreno, J.J. Rocca, Demonstration of a high average power tabletop soft X-Ray Laser, Phys. Rev. Lett. 81 (1998) 5804–5807.
[47] J.H. Chae, D. Kim, Effect of the Cu underlayer on the optoelectrical properties of ITO/Cu thin films, Renew. Energy 35 (2010) 314–317.
[48] G. Haacke, New figure of merit for transparent conductors, J. Appl. Phys. 47 (1976) 4086–4089.